Influence of the buffer layers on magnetic properties of FePt(001) films sputter-deposited at reduced temperature

doi: 10.1063/1.1763000

Influence of the buffer layers on magnetic properties of FePt (001) films sputter-deposited at reduced temperature

T. Seki,[a] T. Shima, K. Takanashi, Y. Takahashi, and E. Matsubara
Institute for Materials Research, Tohoku University, Sendai 980-8577, Japan

Y. K. Takahashi and K. Hono
National Institute for Materials Science, Tsukuba 305-0047, Japan

(Received 23 February 2004; accepted 24 April 2004)

The magnetic properties of $Fe_{38}Pt_{62}$ and $Fe_{52}Pt_{48}$ films sputter deposited on MgO (001) substrates with and without a buffer layer at the substrate temperature T_s of 300 °C have been investigated. Pt, Au, and PtAu alloys with different compositions were used as the buffer layer to study the influence of the lattice mismatch between the FePt layer and the buffer layer. The $L1_0$ ordered structure with large perpendicular magnetic anisotropy has been obtained for the $Fe_{38}Pt_{62}$ films irrespective of the buffer layer. The degree of long-range order S and uniaxial magnetic anisotropy energy K_u increase with increasing the lattice mismatch, and S and K_u show maxima of 0.8 ± 0.1 and 2.7×10^7 erg/cm^3, respectively, for the film without a buffer layer. For $Fe_{52}Pt_{48}$ films, on the other hand, the $L1_0$ ordered structure with perpendicular magnetic anisotropy has been obtained only for the film with an Au buffer layer. © *2004 American Institute of Physics.*
[DOI: 10.1063/1.1763000]

I. INTRODUCTION

For the last decade, the areal density of longitudinal magnetic recording media has dramatically increased and has exceeded 100 Gbit/in.[2] which used to be called the limit of magnetic recording.[1] The ever-increasing demand for higher areal density has pushed the goal up to the Tera bit magnetic recording. In order to realize the ultra high-density magnetic recording, the replacement of the currently used longitudinal magnetic recording system with another one is required. Perpendicular magnetic recording,[2] thermal assisted magnetic recording,[3] and patterned media[4] have been considered as the candidate techniques for the next generation magnetic recording. In these systems, magnetically isolated ferromagnetic particles with a lateral size below 10 nm are needed. However, the instability of magnetization vectors caused by thermal fluctuation is a significant problem for such nanometer sized particles. One of the possible solutions is to use ferromagnetic materials with large uniaxial magnetocrystalline anisotropy.

$L1_0$ ordered FePt alloy with a large uniaxial magnetocrystalline anisotropy ($K_u=7.0\times10^7$ erg/cm^3) (Ref. 5) has attracted much attention because it may overcome the thermal fluctuation at reduced dimensions. Many studies to date have been focused on the fabrication of $L1_0$ ordered FePt thin films with perpendicular anisotropy, considering the application to perpendicular magnetic recording media.[6–12] Although the $L1_0$ ordered structure is thermodynamically stable at room temperature, conventional methods such as sputter deposition or molecular beam epitaxy without heat treatment lead to the formation of the disordered FePt phase with a fcc structure. In order to form the $L1_0$ ordered structure, a high temperature process, e.g., deposition on a heated substrate and/or postannealing above 500 °C, is required. However, this high temperature process is a drawback for practical applications because of a lack of a high temperature durability in currently used materials for hard disk drives. Besides it also accelerates the grain growth in magnetic films leading to the reduction of signal-to-noise ratio in recording media. Several attempts on the low temperature fabrication of FePt films were made: use of proper under layers,[13] addition of third elements,[14,15] annealing of multilayers,[16,17] ion irradiation,[18] alternate monatomic layer deposition,[19] high Ar gas pressure during deposition,[20] and *in situ* annealing.[21]

In a previous paper,[22] we reported that $L1_0$ ordered structure with high perpendicular magnetic anisotropy was obtained for FePt (001) films deposited on Pt buffered MgO (001) substrates even at substrate temperature T_s of 300 °C by shifting the composition of FePt phase to a Pt-rich off-stoichiometric region. Around the stoichiometric $Fe_{50}Pt_{50}$ composition, on the other hand, poor $L1_0$ order and low perpendicular anisotropy were obtained. We have also found that the optimum composition to achieve high $L1_0$ order at $T_s=300$ °C is different depending on the orientation of the epitaxially grown FePt films.[23] These results suggest that the strain from the buffer layer plays a significant role for the formation of the $L1_0$ ordered structure. In other words, it is expected that more highly ordered state may be achieved at low temperature by exploring a proper buffer layer.

In this paper, we have investigated the structures and the magnetic properties of FePt (001) films sputter deposited on MgO (001) substrates at $T_s=300$ °C with and without a buffer layer. As a buffer layer, PtAu alloys with different compositions were used to change the strain arising from the lattice mismatch between the FePt layer and the buffer layer.

[a]Author to whom correspondence should be addressed; electronic mail: gosai@imr.tohoku.ac.jp

The effect of the strain on structures and magnetic properties is also discussed.

II. EXPERIMENTAL PROCEDURE

Samples were prepared on MgO (001) single crystal substrates using a magnetron sputtering apparatus. The base pressure was below 1×10^{-9} Torr, and high-purity argon (>99.9999%) of 5.0 mTorr was flown during sputtering. An Fe seed layer of 1 nm and a buffer layer (Pt, $Pt_{75}Au_{25}$, $Pt_{63}Au_{37}$, or Au) of 40 nm were first deposited at room temperature. The lattice constant of the buffer layer was changed from 0.397 nm of Pt (Ref. 24) to 0.408 nm of Au (Ref. 25), leading to different lattice mismatches between the FePt layer and the buffer layer. Then Fe and Pt were codeposited at $T_s=300\,^{\circ}C$ on the buffer layer. FePt films without an Fe seed and a buffer layer, that is, directly deposited on a MgO substrate were also prepared; the lattice constant of MgO is 0.421 nm,[26] and in this case the lattice mismatch is the largest of all the samples. The FePt layer thickness was fixed to 18 nm. The typical growth rate was 0.01 nm/s. The compositions of FePt layers and buffer layers were determined by electron probe x-ray microanalysis. Two types of samples with different FePt compositions were prepared. One was $Fe_{52}Pt_{48}$ with nearly stoichiometric composition, which showed a disordered phase.[22,27] The other was $Fe_{38}Pt_{62}$ with Pt-rich off-stoichiometric composition, the degree of long-range order and uniaxial magnetic anisotropy of which showed maxima for the film with a Pt buffer layer.[22] X-ray diffraction (XRD) with Cu $K\alpha$ radiation was performed for structural characterization. The conventional 2θ-θ scan was employed to determine the lattice constant in the normal direction to the film plane and the degree of long-range order. In addition, the 2θ-θ scan in the tilted sample was also performed using a four-axes goniometer in order to determine the in-plane lattice constant. The microstructure of the film was observed by transmission electron microscopy (TEM). Magnetization curves were measured by a superconducting quantum interference device magnetometer.

In order to determine the lattice mismatch between the FePt layer and the buffer layer, the lattice constants of a-plane, a_{FePt}, and a_{buffer} are defined in the following way: For a_{buffer} of Pt, Au, and MgO the bulk values are used.[24–26] a_{buffer} of PtAu alloys have been calculated by the Vegard's law[28] using the bulk values of Pt and Au. Although a_{FePt} of fct-FePt could be experimentally obtained from the XRD patterns of the film as shown later, the values of bulk fct-FePt are used in order to evaluate the lattice mismatch comparing the FePt lattice without receiving the strain to the buffer layer. a_{FePt} at each composition has been calculated using that of bulk $Fe_{50}Pt_{50}$ alloy[29] and the Vegard's law.[28] The lattice mismatch $\Delta a/a$ (%) is defined as

$$\Delta a/a=\frac{a_{\mathrm{buffer}}-a_{\mathrm{FePt}}}{a_{\mathrm{buffer}}}\times 100. \tag{1}$$

The values of a and $\Delta a/a$ for $Fe_{38}Pt_{62}$ and $Fe_{52}Pt_{48}$ films with each buffer are summarized in Table I. The values of a_{buffer} are almost equal to those experimentally obtained from the XRD patterns which will be shown later.

TABLE I. Summary of lattice constants a for FePt phases and buffer layers, and the calculated lattice mismatches between the FePt layer and the buffer layer $\Delta a/a$ for the $Fe_{38}Pt_{62}$ and $Fe_{52}Pt_{48}$ films.

	a (nm)	$\Delta a/a$ ($Fe_{38}Pt_{62}$) (%)	$\Delta a/a$ ($Fe_{52}Pt_{18}$) (%)
$Fe_{38}Pt_{62}$ (fcc)	0.383	——	——
$Fe_{52}Pt_{48}$ (fcc)	0.380		
Pt	0.397	3.5	4.3
$Pt_{75}Au_{25}$	0.400	4.2	5.0
$Pt_{63}Au_{37}$	0.401	4.5	5.2
Au	0.408	6.1	6.9
MgO	0.421	9.0	9.7

III. RESULTS AND DISCUSSION

A. Structure

XRD patterns for $Fe_{38}Pt_{62}$ thin films with (a) Pt, (b) $Pt_{75}Au_{25}$, (c) $Pt_{63}Au_{37}$, and (d) Au buffer layers and (e) without a buffer layer are shown in Fig. 1. The unlabeled sharp peaks are due to the MgO substrate. The angles of the 002 and 004 peaks of buffer layers denoted by open circles shift to low angle side by changing the buffer layer materials from a Pt buffer layer to no buffer layer, indicating that different lattice mismatches have been realized by changing the buffer layer materials. The films are strongly textured to the (001) planes, since only 00n diffraction peaks are observed in the patterns. In addition to the fundamental FePt 002 and 004 peaks, the superlattice FePt 001 and 003 peaks associated with the formation of the $L1_0$ ordered structure have been clearly observed for all the samples. The degree of long-range order S has been evaluated from the integrated intensities of XRD fundamental and superlattice peaks extracted by numerical fitting. The detailed procedure for the evaluation of S was described elsewhere.[7,19] The maximum value of $S=0.8\pm0.1$ has been obtained for the film without a buffer layer. The upper limit of S for $Fe_{38}Pt_{62}$ is 0.76.[30] Although the evaluation of S was performed taking into account the structure factor, the Lorentz polarization factor, the Debye-Weller factor, and the decay factor with increasing 2θ angle, a finite error of $\approx\pm0.1$ may remain in S obtained

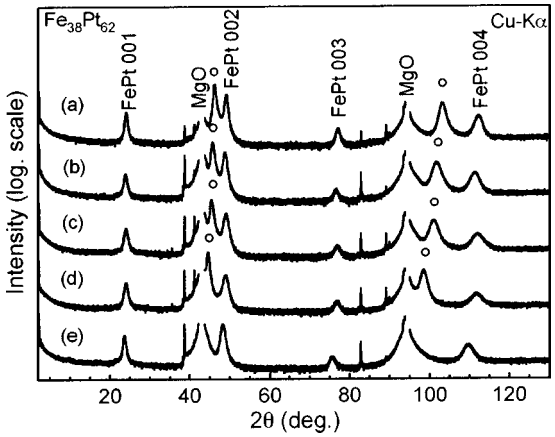

FIG. 1. X-ray diffraction patterns with Cu $K\alpha$ radiation for $Fe_{38}Pt_{62}$ films with (a) Pt, (b) $Pt_{75}Au_{25}$, (c) $Pt_{63}Au_{37}$, and (d) Au buffer layers and (e) without a buffer layer.

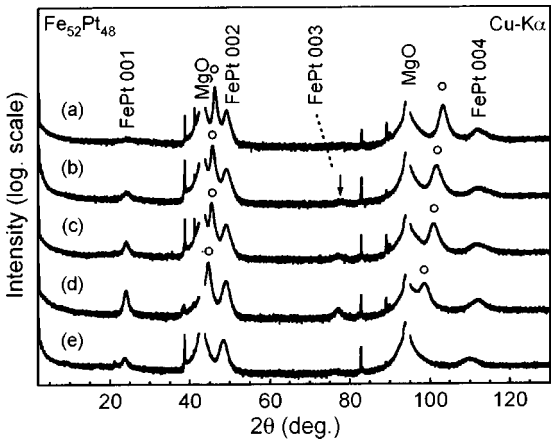

FIG. 2. X-ray diffraction patterns with Cu $K\alpha$ radiation for $Fe_{52}Pt_{48}$ films with (a) Pt, (b) $Pt_{75}Au_{25}$, (c) $Pt_{63}Au_{37}$, and (d) Au buffer layers and (e) without a buffer layer.

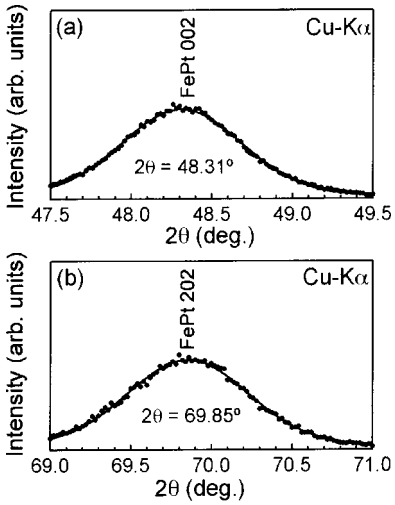

FIG. 3. X-ray diffraction θ-2θ scans around (a) FePt 002 and (b) FePt 202 peaks for the $Fe_{38}Pt_{62}$ film without a buffer layer.

experimentally. The value of S exceeding the upper limit at $Fe_{38}Pt_{62}$ is caused by the error. The values of S are shown with an error bar, and the upper limit is in the range of the error bar.

Figure 2 also shows XRD patterns for $Fe_{52}Pt_{48}$ thin films with (a) Pt, (b) $Pt_{75}Au_{25}$, (c) $Pt_{63}Au_{37}$, and (d) Au buffer layers and (e) without a buffer layer. The preferred crystal orientation of the films is [001] similar to the results of $Fe_{38}Pt_{62}$ films. Only diffuse superlattice peaks are observed for the film with a Pt buffer layer. However, with changing the buffer layer material from Pt to Au, in other words, with increasing the lattice mismatch, the superlattice peaks begin to appear, and the remarkable superlattice peaks are observed for the film with an Au buffer layer. The intensities of superlattice peaks decrease again and the fundamental peaks also become diffused for the film without a buffer layer. It should be noted that the high $L1_0$ order of $S=0.7\pm0.1$ is achieved by changing the buffer layer from Pt to Au even around the stoichiometric composition.

The XRD θ-2θ scans around FePt 002 and 202 peaks were performed using a single crystal diffractometer with high accuracy of $\theta=\pm0.005°$ so as to determine the lattice constants a and c of the FePt layer accurately. As mentioned above, the samples were tilted and 202 diffractions were observed in order to measure the in-plane lattice constant. Figure 3 shows the results of XRD scans around the (a) FePt 002 and (b) 202 peaks for the $Fe_{38}Pt_{62}$ film without a buffer layer. The angles 2θ of FePt 002 and 202 peaks are obtained by Gaussian fitting to be 48.31° and 69.85°, respectively, leading to $a=0.385$ nm and $c=0.377$ nm. Therefore, c/a is calculated to be 0.979, which is larger than 0.964 for stoichiometric bulk $L1_0$ FePt.[29]

Figure 4(a) shows the cross-sectional TEM image for the $Fe_{38}Pt_{62}$ film with a Pt buffer layer. It is confirmed that the FePt layer is grown with continuous morphology on the Pt buffer layer. The enlarged high-resolution electron microscopy image [Fig. 4(b)] clearly shows a misfit dislocation at the FePt/Pt interface. However, excellent crystalline coherency between the Pt buffer and the FePt layers is also confirmed, indicating that the FePt layer is epitaxially grown on the Pt buffer layer.

a and c, c/a, and unit cell volume a^2c as a function of $\Delta a/a$ are summarized in Figs. 5(a), 5(b), and 5(c), respectively. With increasing $\Delta a/a$, a decreases and c increases for both $Fe_{38}Pt_{62}$ and $Fe_{52}Pt_{48}$ films. As a result, c/a tends to increase as $\Delta a/a$ increases. a^2c keeps almost constant regardless of $\Delta a/a$ for each composition. The value of a^2c for the $Fe_{38}Pt_{62}$ film is larger than that for the $Fe_{52}Pt_{48}$ film. Due to a tensile strain between the FePt layer and the buffer layer, c/a was initially expected to decrease with increasing $\Delta a/a$. However, the present results show different behavior from the expectation. The XRD patterns (Figs. 1 and 2) show that the increase of c/a with $\Delta a/a$ does not arise from the formation of the disordered fcc structure. Although the reason for the increase in c/a with $\Delta a/a$ is not clear at present, one possible reason is the effect of an excess number of misfit dislocations at the interface between the FePt layer and the

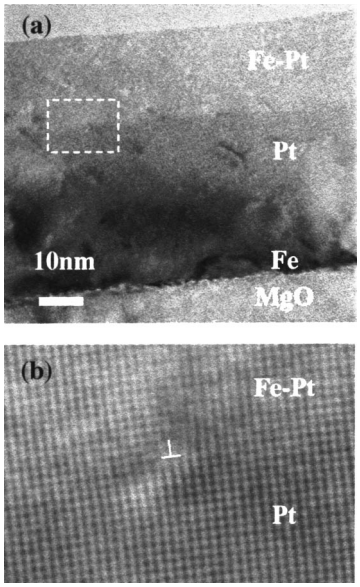

FIG. 4. (a) A cross-sectional TEM image for the $Fe_{38}Pt_{62}$ film with a Pt buffer layer, and (b) the high-resolution electron microscopy image of the enclosed area in (a).

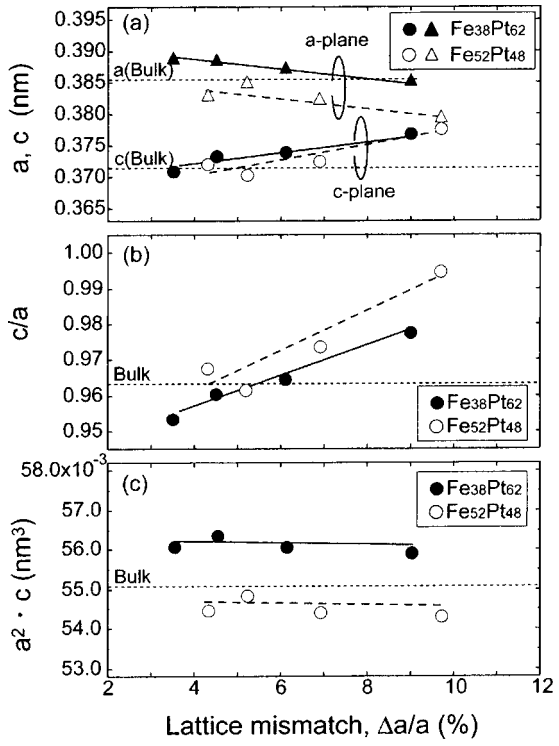

FIG. 5. (a) The lattice constants of a and c, (b) c/a, and (c) the unit cell volume a^2c as a function of the lattice mismatch between the FePt layer and the buffer layer $\Delta a/a$. Solid circles and triangles represent the data for $Fe_{38}Pt_{62}$ films, and open ones represent the data for $Fe_{52}Pt_{48}$ films.

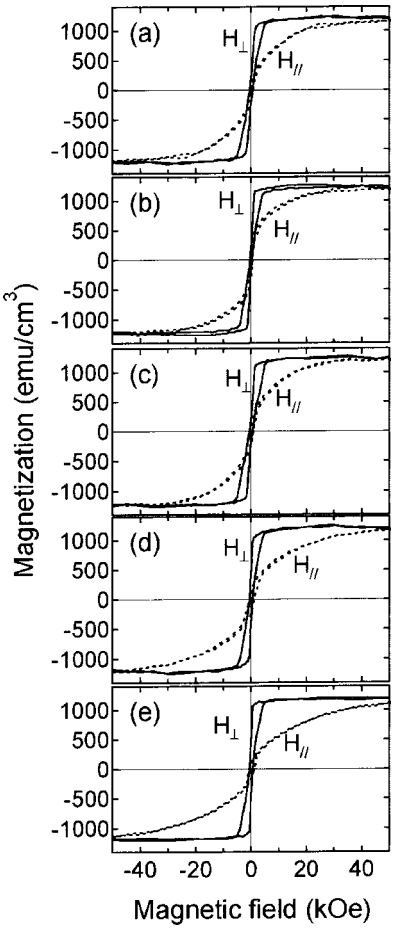

FIG. 6. Magnetization curves for $Fe_{38}Pt_{62}$ films with (a) Pt, (b) $Pt_{75}Au_{25}$, (c) $Pt_{63}Au_{37}$, and (d) Au buffer layers and (e) without a buffer layer. The magnetic field was applied in the perpendicular direction to the film ($H_\perp$: solid curves) and in the in-plane direction ($H_\parallel$: broken curves).

buffer layer. It was shown by the calculation that the strain changes from tensile to compressive depending on the dislocation density in the GaAs/Si heterostructure.[31] Although the quantitative evaluation of the misfit dislocation density is very difficult in the present samples, the films with a large $\Delta a/a$ may receive the compressive strain arising from an excess number of misfit dislocations, leading to the increase of c/a caused by this compressive strain.

B. Magnetic properties

Figure 6 shows the magnetization curves for $Fe_{38}Pt_{62}$ films with (a) Pt, (b) $Pt_{75}Au_{25}$, (c) $Pt_{63}Au_{37}$, and (d) Au buffer layers and (e) without a buffer layer. Solid curves denote the magnetization curves with applied fields perpendicular ($H_\perp$) and broken curves denote those with applied fields parallel ($H_\parallel$) to the film plane. The easy magnetization axis is in perpendicular direction to the film plane for all the samples. This corresponds to the XRD patterns shown in Fig. 1, where the superlattice peaks are clearly observed for all the samples. In particular, the large perpendicular magnetic anisotropy appears in the film without a buffer layer. Uniaxial magnetic anisotropy energy K_u was determined from the area enclosed between the magnetization curves in magnetic fields parallel and perpendicular to the film plane, with the correction of shape anisotropy energy ($-2\pi M_s^2$). The maximum value of $K_u = 2.7\times10^7$ erg/cm^3 has been obtained for the film without a buffer layer.

Figure 7 shows the magnetization curves for $Fe_{52}Pt_{48}$ films with (a) Pt, (b) $Pt_{75}Au_{25}$, (c) $Pt_{63}Au_{37}$, and (d) Au buffer layers and (e) without a buffer layer. The easy magnetization axis lies in the film plane for the film with a Pt buffer layer. As Au concentration in the buffer layer increases, the easy magnetization axis changes from the in-plane to the perpendicular direction. For the film with a Au buffer layer, the easy magnetization direction is perpendicular to the film plane and the value of $K_u = 1.4\times10^7$ erg/cm^3 has been obtained. For the film without a buffer layer, however, K_u decreases again, which corresponds to the decrease in the intensities of superlattice peaks in Fig. 2.

C. Comparison between structure and magnetic properties

S and K_u as a function of $\Delta a/a$ are shown in Figs. 8(a) and 8(b), respectively. Solid and open circles represent the data for $Fe_{38}Pt_{62}$ and $Fe_{52}Pt_{48}$ films, respectively. As $\Delta a/a$ increases, S and K_u increase monotonically for $Fe_{38}Pt_{62}$ films, and the maximum values of $S = 0.8\pm0.1$ and $K_u = 2.7\times10^7$ erg/cm^3 have been obtained for the film without a buffer layer. On the other hand, for $Fe_{52}Pt_{48}$ films, S and K_u increase as $\Delta a/a$ increases, and the maximum value $S = 0.7\pm0.1$ and $K_u = 1.4\times10^7$ erg/cm^3 have been obtained for the film with a Au buffer layer. However, S and K_u decrease for the film without a buffer layer. One possible origin for the increase in S with $\Delta a/a$ is considered as follows: assuming that an excess number of misfit dislocations mentioned in

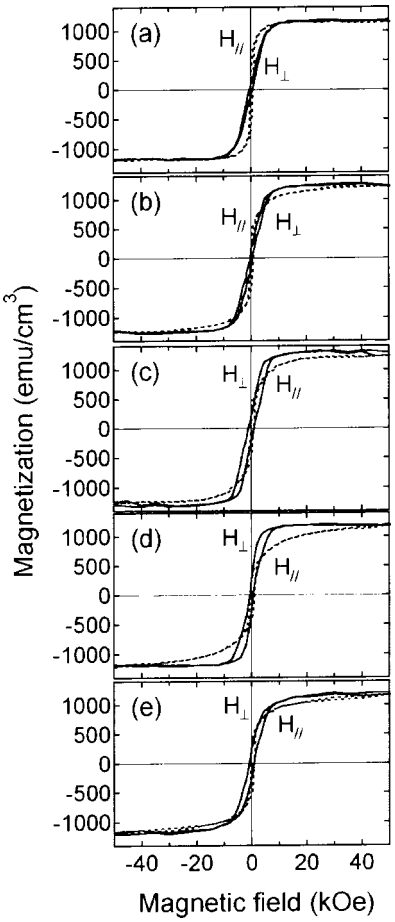

FIG. 7. Magnetization curves for $Fe_{52}Pt_{48}$ films with (a) Pt, (b) $Pt_{75}Au_{25}$, (c) $Pt_{63}Au_{37}$, and (d) Au buffer layers and (e) without a buffer layer. The magnetic field was applied in the perpendicular direction to the film ($H_\perp$: solid curves) and in the in-plane direction ($H_\parallel$: broken curves).

Sec. III A exist in the films, the dislocations are considered to promote the atomic diffusion at low temperature leading to the increase of chemical order. For the $Fe_{52}Pt_{48}$ film without a buffer layer, however, the high $L1_0$ order is not achieved probably because of the too large lattice mismatch. The increase in K_u with S is reasonable, and consistent with the results reported previously.[11,32]

On the other hand, the increase in c/a with S is not consistent with the relationship reported previously:[22] c/a decreased as S increased, and S was evaluated from the value of c/a in the case of bulk alloy[33] or nonepitaxial films.[17] In the present films, S is high; while the crystal structure is elongated along the c-axis direction by the compressive strain induced from the buffer layer. This result suggests that the relationship between S and c/a is not unique in the epitaxial films, but strongly depends on the growth condition. S cannot be always evaluated from c/a.

IV. CONCLUSIONS

In order to discuss the influence of the lattice mismatch between the FePt layer and the buffer layer on the structural and magnetic properties, we prepared FePt (001) films with a variety of buffer layers and without a buffer layer on MgO (001) substrates at $T_s = 300\,^\circ\mathrm{C}$. As the lattice mismatch

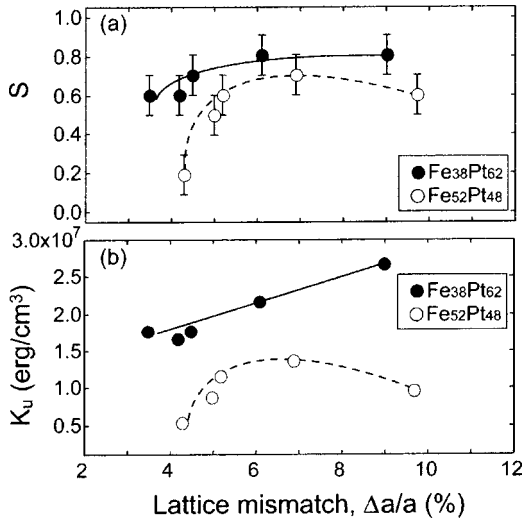

FIG. 8. (a) The degree of long-range order S and (b) uniaxial magnetic anisotropy K_u as a function of the lattice mismatch between the FePt layer and the buffer layer $\Delta a/a$. Solid and open circles represent the data for $Fe_{38}Pt_{62}$ films and $Fe_{52}Pt_{48}$ films, respectively.

$\Delta a/a$ increases, S, K_u, and c/a increase for both $Fe_{38}Pt_{62}$ and $Fe_{52}Pt_{48}$ films. The clear correlation between S and K_u has been found, and is consistent with previous studies. However, the relationship between S and c/a for the epitaxial films is different from the results reported previously. The increase in S with c/a means that the $L1_0$ ordered crystal structure is elongated along the c axis by the compressive strain from the buffer layer. For the epitaxial films, the relationship between S and c/a is not unique. The Pt-rich off-stoichiometric $Fe_{38}Pt_{62}$ films with each buffer layer and without a buffer layer show the $L1_0$ ordered structure with high perpendicular magnetic anisotropy. The maximum values of S and K_u for the $Fe_{38}Pt_{62}$ film without a buffer layer are 0.8 ± 0.1 and 2.7×10^7 erg/cm^3, respectively, whereas, the high S and high perpendicular magnetic anisotropy have been obtained for the $Fe_{52}Pt_{48}$ film with a Au buffer layer. However, for the $Fe_{52}Pt_{48}$ film without a buffer layer, S and K_u decrease because of the too large lattice mismatch. These results indicate that the selection of an adequate combination of the composition and the buffer layer is important to obtain high S and large K_u for FePt (001) films at reduced temperature.

ACKNOWLEDGMENTS

This work was partly supported by the Special Coordination Funds for Promoting Science and Technology on ''Nanohetero Metallic Materials'' from the Ministry of Education, Culture, Sports, Science, and Technology. The structural characterization was performed at Laboratory for Advanced Materials, IMR, Tohoku University. The authors would like to thank Professor S. Mitani, Professor K. Nakajima, and Professor N. Usami for useful discussion and Y. Murakami for technical assistance.

[1] D. Weller and A. Moser, IEEE Trans. Magn. **35**, 4423 (1999).
[2] S. Iwasaki, IEEE Trans. Magn. **16**, 71 (1980).
[3] J. J. M. Ruigrok, J. Magn. Soc. Jpn. **28**, 313 (2001).
[4] R. L. White, R. M. H. New, and R. F. W. Pease, IEEE Trans. Magn. **33**, 990 (1997).
[5] O. A. Ovanov, L. V. Solina, and V. A. Demshina, Phys. Met. Metallogr. **35**, 81 (1973).

[6] B. M. Lairson, M. R. Visokay, R. Sinclair, and B. M. Clemens, Appl. Phys. Lett. **62**, 639 (1993).
[7] A. Cebollada, D. Weller, J. Sticht, G. R. Harp, R. F. C. Farrow, R. F. Marks, R. Savoy, and J. C. Scott, Phys. Rev. B **50**, 3419 (1994).
[8] M. R. Visokay and R. Sinclair, Appl. Phys. Lett. **66**, 1692 (1995).
[9] M. Watanabe and M. Homma, Jpn. J. Appl. Phys. **35**, L1264 (1996).
[10] M. H. Hong, K. Hono, and M. Watanabe, J. Appl. Phys. **84**, 4403 (1998).
[11] S. Okamoto, N. Kikuchi, O. Kitakami, T. Miyazaki, Y. Shimada, and K. Fukamichi, Phys. Rev. B **66**, 024413 (2002).
[12] T. Shima, K. Takanashi, Y. K. Takahashi, and K. Hono, Appl. Phys. Lett. **81**, 1050 (2002).
[13] Yu-Nu Hsu, Sangi Jeong, David E. Laughlin, and David N. Lambeth, J. Appl. Phys. **89**, 7068 (2001).
[14] T. Maeda, T. Kai, A. Kikitsu, T. Nagase, and J. Akiyama, Appl. Phys. Lett. **80**, 2147 (2002).
[15] Y. K. Takahashi, M. Ohnuma, and K. Hono, J. Magn. Magn. Mater. **246**, 259 (2002).
[16] C. P. Luo and D. J. Sellmyer, IEEE Trans. Magn. **31**, 2764 (1995).
[17] Y. Endo, N. Kikuchi, O. Kitakami, and Y. Shimada, J. Appl. Phys. **89**, 7065 (2001).
[18] D. Ravelosona, C. Chappert, V. Mathet, and H. Bernas, Appl. Phys. Lett. **76**, 236 (2000).
[19] T. Shima, T. Moriguchi, S. Mitani, and K. Takanashi, Appl. Phys. Lett. **80**, 288 (2002).
[20] T. Suzuki, K. Harada, N. Honda, and K. Ouchi, J. Magn. Magn. Mater. **193**, 85 (1999).
[21] Y. K. Takahashi, M. Ohnuma, and K. Hono, Jpn. J. Appl. Phys. **40**, L1367 (2001).
[22] T. Seki, T. Shima, K. Takanashi, Y. Takahashi, E. Matsubara, and K. Hono, Appl. Phys. Lett. **82**, 2461 (2003).
[23] T. Seki, T. Shima, K. Takanashi, Y. Takahashi, E. Matsubara, and K. Hono, IEEE Trans. Magn. (submitted).
[24] Powder diffraction file, Inorganic (International Centre of Diffraction Data) PDF# 88-2343.
[25] Powder diffraction file, Inorganic (International Centre of Diffraction Data) PDF# 4-0784.
[26] Powder diffraction file, Inorganic (International Centre of Diffraction Data) PDF# 78-0430.
[27] Y. K. Takahashi, M. Ohnuma, and K. Hono, J. Appl. Phys. **93**, 7580 (2003).
[28] L. Vegard, Zeitschrift fur Physik **5**, 17 (1921).
[29] Powder diffraction file, Inorganic (International Centre of Diffraction Data) PDF# 43-1359.
[30] B. E. Warren, *X-Ray Diffraction* (Dover, New York, 1990) p. 208.
[31] K. Nakajima, J. Cryst. Growth **121**, 278 (1992).
[32] H. Kanazawa, G. Lauhoff, and T. Suzuki, J. Appl. Phys. **87**, 6143 (2000).
[33] B. W. Roberts, Acta Metall. **2**, 597 (1954).